

# Possible non-abelian Moore-Read state in double-layer bosonic fractional quantum Hall system

W. Zhu<sup>1</sup>, S. S. Gong<sup>1</sup>, D. N. Sheng<sup>1</sup>, L. Sheng<sup>2</sup>

<sup>1</sup>*Department of Physics and Astronomy, California State University, Northridge, California 91330, USA*

<sup>2</sup>*National Laboratory of Solid State Microstructures, Department of Physics, and Collaborative Innovation Center of Advanced Microstructures, Nanjing University, Nanjing 210093, China*

Identifying and understanding interacting systems that can host non-Abelian topological phases with fractionalized quasi-particles have attracted intense attention in the past twenty years. Theoretically, it is possible to realize a rich variety of such states by coupling two Abelian fractional quantum Hall (FQH) states together through gapping out part of the low energy degrees of freedom. So far, there are some indications, but no robust examples have been established in bilayer systems for realizing the non-Abelian state in the past. Here, we present a phase diagram of a double-layer bosonic FQH system based on the exact diagonalization and density-matrix renormalization group (DMRG) calculations, which demonstrates a potential regime with the emergence of the non-Abelian bosonic Moore-Read state. Starting from the Abelian phase with four fold topological degeneracy at weak coupling, with the increase of interlayer tunneling, we find an intermediate regime with a three-fold groundstate degeneracy and a finite drag Hall conductance. We find different topological sectors in consistent with Moore-Read state by inserting different fluxes in adiabatic DMRG study. We also extract the modular  $S$ -matrix, which supports the emergence of the non-Abelian Ising anyon quasiparticle in this system.

PACS numbers: 73.43.Cd, 03.65.Ud, 05.30.Pr

## I. INTRODUCTION

The topological states of matter with emergent fractionalized quasiparticles have attracted the intense attentions in the past two decades<sup>1,2</sup>. The statistics of fractionalized quasiparticles fall into two broad categories: Abelian<sup>3</sup> and non-Abelian<sup>4-6</sup>. Interchanging two Abelian quasiparticles changes the groundstates by a non-trivial phase factor, whereas interchanging two non-Abelian quasiparticles rotates the groundstates within a set of degenerated groundstate manifold and the final state will depend on the order of operations being carried out. Since the quasiparticles have unique characterization to a given topological order, it is possible to identify a topological ordered state through the properties of quasiparticles. In particular, compared to the Abelian quasiparticles, the non-Abelian quasiparticles are fundamentally important for our understanding of the emerging physics, which also have potential application for the fault-tolerant topological quantum computation<sup>7,8</sup>. Currently, the most promising platform to investigate the fractional statistics is the fractional quantum Hall (FQH) systems, where most of the observed FQH states carry Abelian quasiparticles. The prominent candidates which may host non-Abelian quasiparticles include the Moore-Read (MR) Pfaffian state<sup>4</sup> at the filling factor  $\nu = 5/2$ <sup>9</sup> and Read-Rezayi (RR) state<sup>6</sup> at  $\nu = 12/5$ <sup>10</sup>, which are the FQH states for electron systems subject to strong magnetic field.

FQH states are also observed in the double-layer systems<sup>11,12</sup>, which can be described in terms of the two-component Halperin states<sup>13,14</sup>. Interestingly, the non-Abelian FQH states may also be realized in the double-layer FQH systems through tuning interlayer tunneling and interactions<sup>15-21</sup>. In such double-layer systems, the Halperin wavefunction upon symmetrization over the layer index indeed shows the characteristic features predicted for the non-Abelian states, including the counting of edge excitations<sup>21</sup> and the quasiholes states<sup>16</sup>. In the theoretical considerations, the non-Abelian state may be induced by increasing the interlayer coupling,

which can gap out the low energy degrees of freedom that are antisymmetric about the layer inversion<sup>17-20,22-26</sup>. However, there are no strong evidence that this mechanism has been realized in physical systems. The numerical studies based on exact diagonalization (ED) on the  $\nu = 1/2$  FQH state for electron systems in double-layer find a large wavefunction overlap between the ground state and the non-Abelian state<sup>27-30</sup>, which is consistent with the symmetrization mechanism of the Halperin wavefunction. However, the obtained energy spectrum has redundant low-energy excitations without a robust energy gap or the groundstate degeneracy on torus geometry<sup>29</sup>, which are not consistent with a non-Abelian QHE state. Very recently, the double-layer bosonic systems on a lattice model with topological flat bands have been studied variationally based on the parton construction and Gutzwiller projected wavefunction. The non-Abelian MR state has been identified by using the topological spin and chiral central charge<sup>32</sup>. However, it remains an open question whether the non-Abelian state is indeed the ground state of the microscopic Hamiltonian. As the possible MR state in this double-layer system appears to be very weak, the accurate simulations for large systems and the systematic numerical characterization of the topological features are highly desired to pin down the nature of the intermediate phase in these systems.

In this paper, we study a bosonic double-layer system<sup>32</sup> with each layer in the  $\nu = 1/2$  Laughlin state in the decoupled limit using the ED and density-matrix renormalization group (DMRG) calculations. With tuning the tunneling and interaction, we find that the four-fold degenerate ground states in the decoupled limit evolve to the three lowest-energy states, which are symmetry states with respect to the layer inversion. These low energy states are separated from the higher energy spectrum by a finite gap in an intermediate parameter regime. To identify the nature of the intermediate phase, we design and perform different flux insertion simulations<sup>33,34</sup>, which can identify total Hall and drag Hall conductances<sup>35</sup>. We find that the intermediate phase is characterized by the

quantized charge Hall conductance and non-zero drag Hall conductance, which is distinguished from the Abelian phase with the quantized charge Hall conductance and zero drag Hall conductance. The flux insertion studies indicate that with growing interlayer tunneling, the system evolves from the two-component Abelian phase to a one-component phase with the nonzero drag Hall conductance, which is consistent with a non-Abelian state. Furthermore, we calculate the modular  $S$ -matrix using ED on finite-size clusters and the obtained  $S$ -matrix fully agrees with that of the MR state.

The remaining of the paper is organized as following: In Sec. II, we introduce the double-layer lattice model built from the topological flat-band (TFB) models. In Sec. III, we present our phase diagram determined by the energy spectrum, charge Hall conductance (Chern number) and drag Hall conductance. In Sec. IV, we present the details of numerical results for the quantum phase diagram. We show the evolution of the energy spectrum with tunneling  $t_\perp$  obtained from ED calculation. The robust groundstate degeneracy is checked by inserting charge and spin fluxes in ED. We further establish the quantum phase diagram based on the newly developed large scale adiabatical DMRG simulations, where we identify the quantized Chern number and finite drag Hall conductance by inserting the fluxes in the possible non-Abelian region. Furthermore, the modular matrix is calculated to support the emergence of non-Abelian Ising anyon in the possible non-Abelian regime. In Sec. V, we discuss the topological trivial phase in our phase diagram. Finally, in Sec. VI, we summarize our main results and discuss open questions.

## II. THEORETICAL MODEL

We consider a double-layer system composed from two single layer topological flat band (TFB) models<sup>36–43</sup>, which can be generally written as:

$$\begin{aligned}\mathcal{H} &= \mathcal{H}_\uparrow + \mathcal{H}_\downarrow + \mathcal{H}_t + \mathcal{H}_U, \\ \mathcal{H}_{\uparrow(\downarrow)} &= - \sum_{(\mathbf{r}\mathbf{r}')} \left[ J_{\mathbf{r}\mathbf{r}'} e^{i\phi_{\mathbf{r}'\mathbf{r}}} b_{\mathbf{r}'\uparrow(\downarrow)}^\dagger b_{\mathbf{r}\uparrow(\downarrow)} + \text{H.c.} \right], \\ \mathcal{H}_t &= t_\perp \sum_{\mathbf{r}} \left[ b_{\mathbf{r}\downarrow}^\dagger b_{\mathbf{r}\uparrow} + \text{H.c.} \right], \\ \mathcal{H}_U &= U_\perp \sum_{\mathbf{r}} n_{\mathbf{r}\downarrow} n_{\mathbf{r}\uparrow},\end{aligned}\tag{1}$$

where  $\mathcal{H}_{\uparrow(\downarrow)}$  denotes the hopping terms in the top layer (bottom layer),  $\mathcal{H}_t$  describes the interlayer tunneling and  $\mathcal{H}_U$  is the interlayer interaction.  $b_{\mathbf{r},s}^\dagger (b_{\mathbf{r},s})$  ( $s = \uparrow$  or  $\downarrow$ ) creates (annihilates) a hard-core boson at site  $\mathbf{r}$ . We consider the TFB model on the square lattice and select the phase factor  $\phi_{\mathbf{r}'\mathbf{r}}$  corresponding to half flux quanta per plaquette<sup>37,39</sup>. The intralayer hopping terms in  $\mathcal{H}_{\uparrow(\downarrow)}$  include the nearest-neighbor coupling  $J_{\langle\mathbf{r}\mathbf{r}'\rangle} = 1.0$  (energy scale), the next-nearest-neighbor coupling  $J_{\langle\langle\mathbf{r}\mathbf{r}'\rangle\rangle} = 0.2941$ , and the next-next-nearest-neighbor coupling  $J_{\langle\langle\langle\mathbf{r}\mathbf{r}'\rangle\rangle\rangle} = -0.2061$ , which give a TFB in each layer with the flatness ratio around 28. Such a model can realize the FQH effect for hardcore bosons

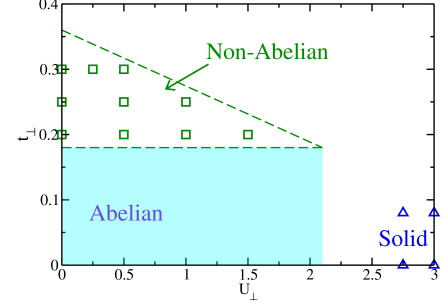


FIG. 1: (Color online) Quantum phase diagram of the double-layer system for the Hamiltonian Eq. (1) with changing the interlayer tunneling  $t_\perp$  and interaction  $U_\perp$ . The blue color filled region represents the topological Abelian phase with the fourfold degenerate ground states and the topological Chern Number  $C^c = 1$ . The green colored squares indicate an intermediate topological order phase with threefold degeneracy and  $C^c = 1$ , which is identified as the one-component non-Abelian Moore-Read state by the finite drag Hall conductance and the modular  $S$ -matrix. The yellow dots represent a solid phase that breaks lattice symmetries.

or interacting fermions without a magnetic field due to the nontrivial Chern number ( $C = 1$ ) carried by the topological band and the reduced kinetic energy<sup>38–42</sup>.

We consider a finite size system with  $2 \times N_x \times N_y$  sites ( $N_x \times N_y$  sites for each layer) and the total filling factor of the lower TFB  $\nu = N_p/N_s = (N_p^\uparrow + N_p^\downarrow)/N_s = 1$ <sup>44,45</sup>, where  $N_p$  is the total number of hardcore bosons and  $N_s$  is the number of single-particle states of the lower TFB. In the following, we will refer the layer index as the (pseudo)spin index for convenience. In the absence of tunneling, the system reduces to the decoupled two layers with each layer at the  $1/2$  filling. While the ED calculations on torus geometry are limited to the system with 40 sites, DMRG<sup>46</sup> allows us to study the systems up to 256 sites on the cylinder which have the periodic boundary in one direction and the open boundary in the other direction. We keep up to  $M = 3600$  states in DMRG calculations, which give accurate results.

## III. PHASE DIAGRAM

Our main results are summarized as the phase diagram in the  $t_\perp - U_\perp$  plane as shown in Fig. 1. We find that the Abelian FQH state of single layer ( $t_\perp = U_\perp = 0$ ) is stable against the weak interlayer tunneling. In the double-layer system, this Abelian phase is characterized by the robust fourfold degenerate ground states, the quantized total charge Chern number  $C^c = 1$ , and the vanishing-small drag Hall conductance. With the increase of interlayer tunneling on finite-size system, the energy of the single antisymmetric ground state splits from the other three symmetrized ground states. The higher energy spectrum has a gap from the threefold symmetrized ground states in an intermediate  $t_\perp$  region (for  $U_\perp = 0$ ,  $0.2 \lesssim t_\perp \lesssim 0.3$ ). In both the Abelian phase and the interme-

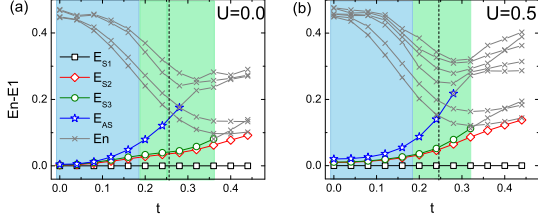


FIG. 2: (Color online) Energy spectrum evolution with the interlayer tunneling  $t_{\perp}$  on  $2 \times 4 \times 4$  torus geometry using ED calculation for (a)  $U_{\perp} = 0.0$  and (b)  $U_{\perp} = 0.5$ . Among the four near degenerating ground states, the three symmetric (S1,S2,S3) states are labeled by the black, green, and red circles, while the anti-symmetric (AS) state is labeled by the blue stars.

diagonal region, we find that the charge Chern Number is always quantized as  $C^c = 1$ ; however, the drag Hall conductance jumps from the vanishing-small value in the Abelian phase to the almost saturated value in the intermediate region, indicating that the system evolves from a two-component to a one-component QHE state. The phase boundary between Abelian and the possible non-Abelian phase is determined by drag Hall conductance reaching half of its saturated value ( $\sim 0.125$ ) based on DMRG simulation. Interestingly, using the threefold ground states, we extract the modular  $\mathcal{S}$ -matrix, which supports a non-Abelian MR state with the emergent Ising anyon quasiparticle and the corresponding fusion rule. In the larger tunneling regime ( $t_{\perp} > 0.3$ ), the system becomes a topologically trivial state with vanishing Chern numbers ( $C^c = 0$ ). In the large  $U_{\perp}$  region, we find a charge density wave state that breaks lattice symmetries.

#### IV. TOPOLOGICAL NONTRIVIAL QUANTUM HALL PHASES

##### A. Energy spectrum on torus

We first use ED to study the evolution of energy spectrum with tunneling  $t_{\perp}$  at  $U_{\perp} = 0$  on the  $2 \times 4 \times 4$  torus system. At  $t_{\perp} = 0$ , both layers have the bosonic  $\nu = 1/2$  Laughlin states with twofold degenerate ground states. Thus, the energy spectrum of the whole system has a fourfold degeneracy separated from higher energy levels by a robust gap. As the double layer system has a layer inversion symmetry<sup>19,29-31</sup>, the fourfold ground states can be divided into two groups: the symmetric group with three states  $E_{S1}, E_{S2}, E_{S3}$  shown as open circles and the anti-symmetric group with a single state  $E_{AS}$  represented by blue stars as shown in Fig. 2. By increasing the interlayer tunneling, the groundstate degeneracy is lifted gradually. The energy of the anti-symmetric state grows rapidly and merges into the high energy continuum at  $t_{\perp} \approx 0.25$ . With further increasing  $t_{\perp}$ , two of the three symmetric states also merge into high energy continuum at  $t_{\perp} \approx 0.36$ . In the intermediate regime  $0.20 \lesssim t_{\perp} \lesssim 0.36$ , the three symmetric states have close energies separating from the

higher energy anti-symmetric state by a finite gap. Although there is a finite splitting between the lowest three states due to the finite size effect allowing topological distinct states being coupled together, the low-energy spectrum of the intermediate region implies a possible threefold degenerate ground states protected by a gap in the thermodynamic limit. In the presence of interlayer interaction, we observe the similar results as shown in Fig. 2(b) for  $U_{\perp} = 0.5$ . Thus, the phase region with  $t_{\perp} \approx 0.25$ , which has the maximum finite-size gap, may be the suitable phase regime for observing the possible non-Abelian Moore-Read state.

##### B. Flux insertion based on ED

We check whether the threefold degeneracy is robust by considering the response of the low-energy spectrum to the flux insertion. To induce the flux, we impose a twisted boundary condition in the  $\hat{y}$ -direction:  $\langle \mathbf{r}_i + N_y \hat{y} | \Psi_{\theta_y} \rangle = \langle \mathbf{r}_i | e^{i\theta_y \sigma_{0(3)}} | \Psi_{\theta_y} \rangle$ , where  $\Psi_{\theta_y}$  is the many-body state with boundary phase  $\theta_y$  and Pauli matrix  $\sigma_{0(3)}$  acts on the layer degrees of freedom of the particle at the position  $r_i$ . The twisted boundary is equivalent to threading a flux in the hole of a torus along the  $\hat{x}$ -direction<sup>47</sup>. In the double-layer system, we introduce two kinds of boundary conditions: charge flux ( $\sigma_0$ ) and spin flux ( $\sigma_3$ )<sup>35,48,49</sup>. In the charge and spin flux, the boundary phases in the top and bottom layers have the same ( $\theta_y^{\uparrow} = \theta_y^{\downarrow}$ ) and the opposite ( $\theta_y^{\uparrow} = -\theta_y^{\downarrow}$ ) signs, respectively. For the topological states, the degenerate ground states should remain gapped without level crossing with the higher energy levels in the charge flux insertion. Therefore, the charge flux insertion can be used to identify the near degenerate ground states from the low-energy levels. Furthermore, it is expected that a two-component double-layer system will have similar responses to the charge and spin fluxes, while a coupled one-component system has the different responses.

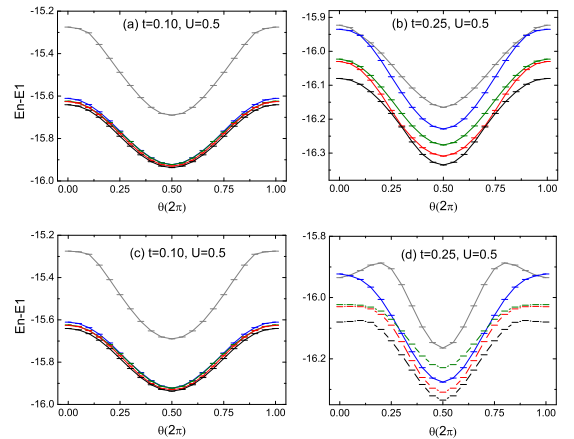


FIG. 3: (Color online) Energy spectrum evolution with (a-b) inserting a charge flux  $\theta_y^{\uparrow} = \theta_y^{\downarrow}$  and (c-d) a spin flux  $\theta_y^{\uparrow} = -\theta_y^{\downarrow}$  for  $(t_{\perp}, U_{\perp}) = (0.1, 0.5)$  and  $(t_{\perp}, U_{\perp}) = (0.25, 0.5)$ . The lowest five energy levels are shown.



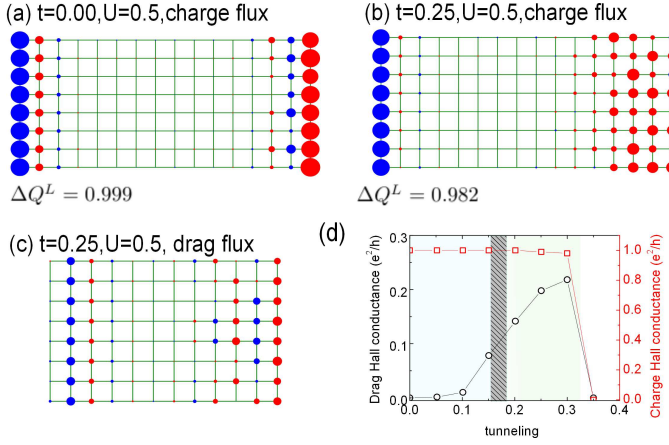


FIG. 4: (Color online) Real-space configuration of charge accumulation  $\langle n_i^\uparrow + n_i^\downarrow \rangle$  after adiabatically inserting a unit charge flux  $\theta_y^\uparrow = \theta_y^\downarrow = 2\pi$  for (a)  $(t_\perp, U_\perp) = (0.00, 0.5)$  and (b)  $(0.25, 0.5)$ . The area of the circle is proportional to the accumulation amplitude and the red (blue) color represents the positive (negative) value. The results are calculated on  $2 \times 8 \times 16$  cylinder using DMRG by keeping 3600 states. (c) Real-space configuration of charge accumulation  $\langle n_i^\uparrow \rangle$  after adiabatically inserting a quantized drag flux  $\theta_y^\uparrow = 2\pi$  ( $\theta_y^\downarrow = 0$ ). (d) The Charge Hall conductance (red squares) and drag Hall conductance (black circles) versus tunneling  $t_\perp$ . The results for drag flux are calculated on  $2 \times 8 \times 12$  cylinder using DMRG by keeping 3600 states.

Fig. 3 shows the ED results of the evolution of low-energy spectra with inserting charge and spin fluxes for the system with weak and intermediate tunnelings. For  $t_\perp = 0.10$  and  $U_\perp = 0.5$ , the four lowest-energy states are always protected by a gap with tuning the charge (Fig. 3(a)) or the spin flux (Fig. 3(c)), which are consistent with a two-component topological state with fourfold degeneracy. In the possible non-Abelian phase for  $(t_\perp, U_\perp) = (0.25, 0.5)$ , the lowest three energy levels are always separated from the higher energy spectrum by a small gap in the charge flux insertion (Fig. 3(b)). By inserting a spin flux (Fig. 3(d)), we find that the lowest three levels connect with higher energy states. These observations indicate that the intermediate region is a strongly coupled one-component topological state with threefold degeneracy. However, the nature of the intermediate regime can not be established based on these ED calculations. As shown in the phase diagram Fig. 1, we determine the phase boundary of the Abelian phase where the fourfold degeneracy of energy spectrum is being destructed, and a possible non-Abelian phase may emerge. We will present the full evidence of the nature of the non-Abelian state below.

### C. Flux insertion based on DMRG

To further investigate the topological properties of the double-layer system on larger size, we use DMRG to study the cylinder system by adiabatically threading a charge or drag flux. The drag flux is realized by introducing the twist boundary phase in just one layer, which can induce a Hall response

in its own layer and also drag the particles in the other layer. Theoretically, the drag Hall conductance and its connection to the topological Chern number matrix<sup>35,47,48</sup> has been established before. Conventionally, one obtains such topological Chern invariants based on ED calculations<sup>35,48</sup>. Very recently, the flux insertion has been introduced in the large-scale DMRG simulation on cylinder systems<sup>51–53</sup>, which can be used to detect different Hall conductances.

Very interestingly, the inserting fluxes method we establish here for double layer systems can also be used to access all the topological sectors in the system. This argument can be easily understood in the decoupled limit. Starting from the ground state without any flux, we insert the charge flux by adiabatically increasing the twist boundary phase in the closed boundary along the  $y$  axis  $\theta_y^\uparrow = \theta_y^\downarrow = 0 \rightarrow 2\pi$ . By inserting  $2\pi$  flux, the ground state of each layer evolves into a new topological sector with a fractional  $1/2$  charged quasi-particle being pumped from one edge of cylinder to the other one<sup>52</sup>. Then, by adding the drag flux in either layers separately, the system would evolve to the other two sectors, which has one more pumped charge  $1/2$  quasi-particle in the layer with drag flux. Therefore, we obtain the four topological degenerate ground states in the Abelian phase. Qualitatively, this picture in the decoupled limit applies to the whole Abelian phase as long as the drag Hall conductance is vanishing small, i.e., one layer cannot effectively drag the other layer. When the system has a transition from two components to one component<sup>50</sup>, the drag Hall conductance would jump to a finite value close to the saturated value. In the coupled one-component system, the drag flux applied to either one of the layer will evolve the system to the same topological sector by pumping one fractional charged quasiparticle, thus we only obtain three topological sectors for coupled phase.

As shown in Fig. 4(a), after the insertion of one charge flux quantum ( $\theta_y^\uparrow = \theta_y^\downarrow = 0 \rightarrow 2\pi$ ), a net quantized charge (boson number) accumulates at the left edge ( $n_c^\uparrow + n_c^\downarrow \approx 0.999$  is the net charge accumulation). The charge accumulation is equivalent to a net charge transfer from the right edge to the left edge. According to the fundamental correspondence between edge transfer and bulk Chern number<sup>34</sup>, we find a quantized charge Chern number  $C^c = 1$  for this Abelian FQH state.

The quantized charge transfer also persists in the possible non-Abelian parameter region. As shown in Fig. 4(b), the net charge transfer corresponds to a quantized charge Chern number  $C^c = 1$ , which indicates the topological nontrivial nature of the possible non-Abelian phase. Nevertheless, the charge flux cannot distinguish the Abelian phase from the possible non-Abelian phase since both of them share the same  $C^c = 1$ . To further identify the phase transition between the Abelian phase and the possible non-Abelian phase, we consider the effects of the drag flux.

By threading a drag flux quantum in the top layer ( $\theta_y^\uparrow = 0 \rightarrow 2\pi$ ,  $\theta_y^\downarrow = 0$ ), we observe the particle accumulations in the bottom layer<sup>35,50</sup> as shown in Fig. 4(c)). By calculating the drag Hall conductance as a function of  $t_\perp$  as displayed in Fig. 4(d), we find a strong enhancement of drag Hall conductance at  $t_\perp \simeq 0.15$ , which coincides with the phase boundary of the disappearance of the Abelian phase identified

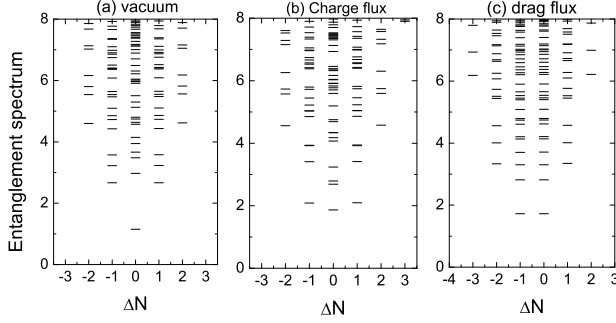


FIG. 5: (Color online) The entanglement spectrum for  $t_{\perp} = 0.25, U_{\perp} = 0.0$  on the  $L_y = 8$  cylinder with (a) no flux, (b) a charge flux quanta, and (c) a drag flux (flux imposed on one layer only). The entanglement spectrum are grouped by the relative boson number  $\Delta N$  of left half cylinder. The results are obtained using DMRG by keeping up to 1600 states.

from the ED energy spectrum calculations. Within the regime  $0.25 \lesssim t_{\perp} \lesssim 0.30$ , the drag Hall conductance approaches the saturated value 0.25, which is consistent with an effective one-component system. Based on the above results, we determine the Abelian phase (blue color), the one-component non-Abelian phase (green squares) as shown in Fig. 1. The topological trivial solid phase with zero charge Chern number is also shown.

To further identify the possible non-Abelian state, we investigate the entanglement spectra of each topological sector. Physically, the different topological ground states on a cylinder are expected to have the different well-defined anyonic flux through the cylinder. Thus, the cylinder system with the charge flux or the drag flux corresponds to the other two topologically distinct ground states besides the vacuum state. To explicitly demonstrate the ground states with different anyonic flux on cylinder geometry, we bipartite the cylinder into two halves, and observe entanglement spectrum<sup>54</sup> to distinguish the different topological sectors. As shown in Fig. 5, we show the entanglement spectrum for the vacuum ground state in Fig. 5(a), the new ground state obtained by inserting a charge flux quantum in Fig. 5(b), and the ground state obtained by inserting a drag flux in Fig. 5(c). These three ground states are anticipated to have one-to-one correspondence with identity, fermion, and Ising anyon sectors, respectively. We also calculate the momentum dependence of the entanglement spectra in each  $U(1)$  quantum number sector with different relative boson number  $\Delta N$ , and obtain the counting of the leading eigenvalues in the entanglement spectra<sup>62</sup>. The obtained results are similar to those of coupled two Laughlin  $\nu = 1/2$  states. Due to the calculation limit,  $N_x = 8$  (16 lattice sites in the  $\hat{x}$  direction) is the largest width we can reach convergence in our DMRG calculations, which gives four momentum quantum numbers  $K = 0, \pi/2, \pi, 3\pi/2$  in each  $\Delta N$  sector. Although we observe that a very small entanglement gap opens up in  $K = \pi$  and  $3\pi/2$  sectors between the expected counting for non-Abelian MR state and the other part of entanglement spectrum, we cannot determine if the gap will survive in the thermodynamic limit or it is a finite size effect.

Since all other results support the non-Abelian QHE state, we believe this result is due to the finite size effect and we leave this part for the future study.

#### D. Modular matrix

From the above observation of DMRG, we find that the intermediate phase region appears as a one-component topological nontrivial phase. Here we calculate the modular  $\mathcal{S}$ -matrix using the near degenerate threefold states in the ED energy spectrum to further investigate the nature of the possible non-Abelian phase<sup>1</sup>. Modular  $\mathcal{S}$ -matrix encodes the information of the quasiparticle statistics including quantum dimension and fusion rules<sup>56–58</sup>, which has been successfully used to identify various Abelian and non-Abelian topological orders<sup>59–65</sup>. To calculate the modular matrix, we follow the method based on the minimal entangled states (MESs)<sup>60</sup>. The MESs are the eigenstates of the Wilson loop operators with a definite type of quasiparticle<sup>59</sup>. Thus, the modular transformations on the MESs give rise to the modular matrix<sup>60</sup>.

Here we show the results at  $t_{\perp} = 0.25, U_{\perp} = 0.0$  as an example. We denote the three lowest-energy states in ED spectrum as  $|\xi_j\rangle$  ( $j = 1, 2, 3$ ), from which we can form the general superposition states as,

$$|\Psi_{(c_2, c_3, \phi_2, \phi_3)}\rangle = c_1|\xi_1\rangle + c_2e^{i\phi_2}|\xi_2\rangle + c_3e^{i\phi_3}|\xi_3\rangle$$

where  $c_1, c_2, c_3, \phi_2, \phi_3$  are real superposition parameters. For each state  $|\Psi\rangle$ , we construct the reduced density matrix and obtain the corresponding entanglement entropy. To find the MESs, we optimize the superposition parameters to find the minimum entanglement entropy. As shown in Fig. 6(a), we show the entropy profile of  $|\Psi\rangle$  with the optimized parameters ( $\phi_2^o, \phi_3^o$ ) for the middle cut along the  $x$ -direction. We find the first global MES  $|\Xi_1^I\rangle$  with the entropy  $S \sim 3.10$  at the position pointed by the red arrow. The second MES  $|\Xi_2^I\rangle$  (blue arrow) and the third MES  $|\Xi_3^I\rangle$  (green arrow) can be determined in the state space orthogonal to  $|\Xi_1^I\rangle$ , as shown in Fig. 6(b). Finally, we can obtain the modular matrix  $\mathcal{S} = \langle \Xi^I | \Xi^I \rangle$  ex-

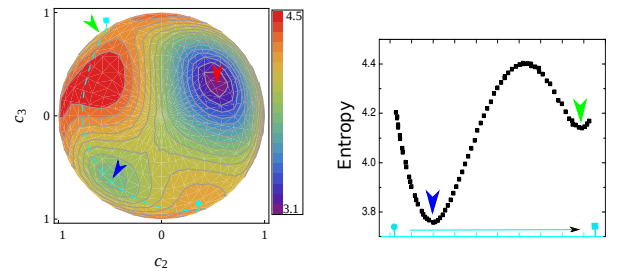


FIG. 6: (Color online) Left: Contour plot of entanglement entropy of  $|\Psi_{c_1, c_2, c_3, \phi_2, \phi_3}\rangle$  on  $2 \times 4 \times 4$  system. We show entropy profile versus  $c_2, c_3$  ( $c_1 = \sqrt{1 - c_2^2 - c_3^2}$ ) by setting optimized  $\phi_2^o, \phi_3^o$ . Three nearly orthogonal MESs are marked by red, green and blue arrows in surface plot. The cyan dashed line represents the states orthogonal to the first MES (red arrow). Right: Entropy for the states along the cyan dashed line as shown in left figure.

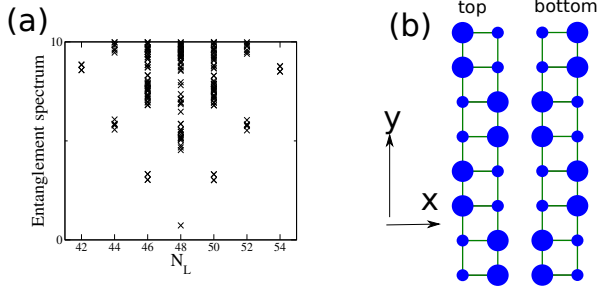


FIG. 7: (Color online) (a) Entanglement spectrum for  $t_{\perp} = 0.08$ ,  $U_{\perp} = 1.2$ . (b) The charge density distribution of  $\langle n_i^{\uparrow} \rangle$  (top layer) and  $\langle n_i^{\downarrow} \rangle$  (bottom layer) in real-space. Here we only show two columns in the bulk in each layer. The two-column pattern is periodic along the cylinder direction. The area of the circle is proportional to the amplitude of charge density. The results are calculated on the  $2 \times 8 \times 16$  cylinder using DMRG with keeping 1600 states.

tracted from the overlap between the MESs for two noncontractible partition cut directions<sup>60</sup>:

$$\mathcal{S} \approx \mathcal{S}^{CS} + \Delta\mathcal{S} = \frac{1}{2} \begin{pmatrix} 1 & 1 & \sqrt{2} \\ 1 & 1 & -\sqrt{2} \\ \sqrt{2} & -\sqrt{2} & 0 \end{pmatrix} + 10^{-2} \times \begin{pmatrix} -5.6 & 5.4 & 1.4 \\ 5.4 & -2.5 & 3.2 \\ 1.4 & 3.2 & 6.2 \end{pmatrix},$$

where  $\mathcal{S}^{CS}$  represents the theoretical prediction from the  $SU(2)_2$  Chern-Simons theory<sup>57–59</sup>.  $\mathcal{S}^{CS}$  determines the quasiparticle quantum dimension as  $d_{\mathbb{1}} = 1$ ,  $d_{\psi} = 1$ ,  $d_{\sigma} = \sqrt{2}$  and non-trivial fusion rule as  $\sigma \times \sigma = \mathbb{1} + \psi$ , where  $\mathbb{1}$  represents the identity particle,  $\psi$  the fermion-type quasiparticle,  $\sigma$  the Ising anyon quasiparticle. Thus, the numerical extracted modular  $\mathcal{S}$ -matrix identifies the intermediate topological phase with threefold ground state degeneracy as the non-Abelian MR state with the emergence of the Ising anyon quasiparticles satisfying the non-Abelian fusion rule ( $\mathcal{S}_{33} \approx 0$ )<sup>61,65</sup>.

Generally speaking, to uniquely determine a topological order, one needs both the modular  $\mathcal{S}$  and  $\mathcal{U}$  matrices<sup>60</sup>. From modular  $\mathcal{U}$  matrix, one can access the chiral central charge  $c$  and topological spin of each quasiparticle, which distinguish the non-Abelian MR state from double-layer Abelian Laughlin states. For example, the chiral central charge of non-Abelian MR state is  $c = 3/2$ , while the double-layer Laughlin state has  $c = 2$ . Unfortunately, in the current lattice model (in Eq. 1), the MES route can not give the  $\mathcal{S}$  and  $\mathcal{U}$  matrix together since there is no rotation  $\pi/3$  symmetry here<sup>60</sup>. Recently, we note that it has been proposed a general method, named momentum polarization<sup>32</sup>, to extract the quasiparticle statistics in modular  $\mathcal{U}$  matrix. In this method, one needs to perform a finite-size scaling on  $L_y$ , then the statistics information in modular  $\mathcal{U}$  matrix can be extracted from  $L_y \rightarrow 0$  limit. Unfortunately, in current DMRG calculation we are limited to the system sizes  $L_y = 4, 6, 8$  due to the computational capability. Thus a reliable application of momentum polarization method here is very challenging, which we leave for the future study.

## V. TOPOLOGICAL TRIVIAL PHASES

Besides the two topological non-trivial phases in the phase diagram Fig. 1, we also find the topological trivial phases at the large  $U_{\perp}$  parameter region. Here we show that there is a charge density wave phase at large  $U_{\perp}$  region, as shown by the yellow triangular in Fig. 1. As shown in Fig. 7(a), the entanglement spectrum has a large weight on the lowest eigenvalue, which is a feature of a solid phase. In Fig. 7(b), we demonstrate the charge density wave pattern in real space. Along the cylinder axis ( $x$ -direction), the unit cell (enclosing 4 sites) is doubled in each layer due to the charge density pattern. In the  $y$ -direction, the charge density pattern has a period of two. At each site, the top and bottom layers have the opposite density pattern, which leaves  $\langle n_i^{\uparrow} + n_i^{\downarrow} \rangle$  a constant.

## VI. SUMMARY AND DISCUSSION

We have studied a bosonic double-layer system on a square lattice using ED and DMRG calculations. Through the studies of the energy spectrum, the flux insertion on cylinder, and the modular matrix, we find numerical evidences for a non-Abelian Moore-Read state emerging from the bilayer Halperin states through gapping out the interlayer anti-symmetric state. Although this practically powerful route to a variety of non-Abelian quantum states has been introduced theoretically for decades based on parton construction and field theory<sup>17–20,22–26</sup>, there were limited numerical evidence to support the realization of non-Abelian state in microscopic systems. Our numerical calculations rely on the insertion of charge and drag fluxes, which allow us to detect the quantum phase transition from a two-component topological state to a one-component state characterized by the onset of the finite drag Hall conductance. In combining with the modular matrix simulation for the quasiparticle statistics, we identify the nature of the intermediate  $t_{\perp}$  (with threefold near degeneracy) phase as the non-Abelian Moore-Read state, although this state is relatively weak and the entanglement spectrum does not show a robust entanglement spectrum gap for the counting associated with the non-Abelian state.

We have also explored the nature of the quantum phase transition between the Abelian phase and the possible non-Abelian phase. We have studied quantities such as entanglement entropy and the wavefunction overlap. We find all of these quantities of the groundstate change smoothly when the system crosses the phase boundary. This indicates that the phase transition is either weakly first order or continuous transition. Moreover, it would be particularly interesting to study the possibility of realizing the non-Abelian phase from coupled bilayer Halperin states in fermionic systems, which will be investigated in the future work.

*Note added.* Upon finalizing the manuscript we noticed several preprints focusing on double-layer  $\nu = 1/3 + 1/3$  fermionic systems<sup>67–70</sup>.



## VII. ACKNOWLEDGEMENTS

WZ thanks Y. Zhang and N. Regnault for insightful comments. This work is supported by the U.S. Department of Energy, Office of Basic Energy Sciences under Grant

No. DE-FG02-06ER46305 (WZ, DNS), the NSF grant DMR-1408560 (SSG), the State Key Program for Basic Researches of China under grants numbers 2015CB921202, 2014CB921103, and the National Natural Science Foundation of China under grant numbers 11225420 (LS).

- 
- <sup>1</sup> X. G. Wen, Int. J. Mod. Phys. B **4**, 239 (1990).
  - <sup>2</sup> A. Stern, Nature **464**, 187 (2010).
  - <sup>3</sup> R. B. Laughlin, Phys. Rev. Lett. **50**, 1395 (1983).
  - <sup>4</sup> G. Moore and N. Read, Nucl. Phys. B **360**, 362 (1991).
  - <sup>5</sup> M. Greiter, X. G. Wen and F. Wilczek, Phys. Rev. Lett. **66**, 3205 (1991).
  - <sup>6</sup> N. Read and E. Rezayi, Phys. Rev. B **59**, 8084 (1999).
  - <sup>7</sup> A. Y. Kitaev, Ann. Phys. **303**, 2 (2003).
  - <sup>8</sup> C. Nayak, S. H. Simon, A. Stern, M. Freedman and S. D. Sarma, Rev. Mod. Phys. **80**, 1083 (2008).
  - <sup>9</sup> R. Willett, J. P. Eisenstein, H. L. Stormer, D. C. Tsui, A. C. Gosard and J. H. English, Phys. Rev. Lett. **59**, 1776 (1987).
  - <sup>10</sup> J. S. Xia, W. Pan, C. L. Vicente, E. D. Adams, N. S. Sullivan, H. L. Stormer, D. C. Tsui, L. N. Pfeiffer, K. W. Baldwin, and K. W. West, Phys. Rev. Lett. **93**, 176809 (2004).
  - <sup>11</sup> J. P. Eisenstein, G. S. Boebinger, L. N. Pfeiffer, K. W. West and S. He, Phys. Rev. Lett. **68**, 1383 (1992).
  - <sup>12</sup> Y. W. Suen, L. W. Engel, M. B. Santos, M. Shayegan and D. C. Tusi, Phys. Rev. Lett. **68**, 1379 (1992).
  - <sup>13</sup> B. I. Halperin, Helv. Phys. Acta **56**, 75 (1983).
  - <sup>14</sup> B. I. Halperin, Surf. Sci. **305**, 1 (1994).
  - <sup>15</sup> T. L. Ho, Phys. Rev. Lett. **75**, 1186 (1995).
  - <sup>16</sup> C. Nayak, F. Wilczek, Nucl. Phys. B **479**, 529-553 (1996).
  - <sup>17</sup> E. Fradkin, C. Nayak, K. Schoutens, Nucl. Phys. B **546**, 711 (1999).
  - <sup>18</sup> X. G. Wen, Phys. Rev. B **60**, 8827 (1999).
  - <sup>19</sup> N. Read and D. Green, Phys. Rev. B **61**, 10267 (1999).
  - <sup>20</sup> X. G. Wen, Phys. Rev. Lett. **84**, 3950 (2000).
  - <sup>21</sup> E. Rezayi, X. G. Wen and N. Read, arXiv:1007.2022 (2010).
  - <sup>22</sup> M. Barkeshli and X. G. Wen, Phys. Rev. B **84**, 115121 (2011).
  - <sup>23</sup> A. Cappelli, L. S. Georgiev, I. T. Todorov, Commun.Math.Phys. **205**, 657-689 (1999).
  - <sup>24</sup> A. Cappelli, L. S. Georgiev, and I. T. Todorov, Nucl. Phys. B **599**, 499 (2001).
  - <sup>25</sup> D. C. Cabra, A. Lopez and G. L. Rossini, Eur. Phys. J. B. **19**, 21-24 (2001).
  - <sup>26</sup> A. Vaezi and M. Barkeshli, Phys. Rev. Lett. **113**, 236804 (2014).
  - <sup>27</sup> N. Regnault, M. O. Goerbig, and Th. Jolicoeur, Phys. Rev. Lett. **101**, 066803 (2008).
  - <sup>28</sup> N. Read and E. Rezayi, Phys. Rev. B **54**, 16864 (1996).
  - <sup>29</sup> Z. Papic, M. O. Goerbig, N. Regnault, and M. V. Milovanovic, Phys. Rev. B **82**, 075302 (2010).
  - <sup>30</sup> M. R. Peterson, Z. Papic, and S. Das Sarma, Phys. Rev. B **82**, 235312 (2010).
  - <sup>31</sup> K. Nomura and D. Yoshioka, J. Phys. Soc. Jpn. **73**, 2612(2004).
  - <sup>32</sup> Y. Zhang, and X. L. Qi, Phys. Rev. B **89**, 195144 (2014).
  - <sup>33</sup> R. B. Laughlin, Phys. Rev. B **23**, 5632 (R) (1981).
  - <sup>34</sup> R. E. Prange and S. M. Girvin, *The quantum Hall effect*, Springer (Berlin, 1987).
  - <sup>35</sup> D. N. Sheng, L. Balents and Z. Wang, Phys. Rev. Lett. **91**, 116802 (2003).
  - <sup>36</sup> F. D. M. Haldane, Phys. Rev. Lett. **61**, 2015 (1988).
  - <sup>37</sup> E. Kapit and E. Mueller, Phys. Rev. Lett. **105**, 215303 (2010).
  - <sup>38</sup> E. Tang, J. W. Mei and X. G. Wen, Phys. Rev. Lett. **106**, 236802 (2011).
  - <sup>39</sup> T. Neupert, L. Santos, C. Chamon and C. Mudry, Phys. Rev. Lett. **106**, 236804 (2011).
  - <sup>40</sup> K. Sun, Z. C. Gu, H. Katsura and S. Das Sarma, Phys. Rev. Lett. **106**, 236803 (2011).
  - <sup>41</sup> D. N. Sheng, Z. C. Gu, K. Sun and L. Sheng, Nature Commun. **2**, 389 (2011).
  - <sup>42</sup> N. Regnault and B. A. Bernevig, Phys. Rev. X **1**, 021014 (2011).
  - <sup>43</sup> Y.-F. Wang, H. Yao, Z.-C. Gu, C.-D. Gong, and D. N. Sheng, Phys. Rev. Lett. **108**, 126805 (2012).
  - <sup>44</sup> N. R. Cooper, N. K. Wilkin, and J. M. F. Gunn, Phys. Rev. Lett. **87**, 120405 (2001).
  - <sup>45</sup> N. Regnault and T. Jolicoeur, Phys. Rev. Lett. **91**, 030402 (2003).
  - <sup>46</sup> S. R. White, Phys. Rev. Lett. **69**, 2863 (1992).
  - <sup>47</sup> Q. Niu, D. J. Thouless, and Y. S. Wu, Phys. Rev. B **31**, 3372 (1985).
  - <sup>48</sup> D. N. Sheng, Z. Y. Weng, L. Sheng and F. D. M. Haldane, Phys. Rev. Lett. **97**, 036808 (2006).
  - <sup>49</sup> T. Neupert, L. Santos, S. Ryu, C. Chamon, and C. Mudry, Phys. Rev. B **84**, 165107 (2011).
  - <sup>50</sup> K. Yang and A. H. MacDonald, Phys. Rev. B **63**, 073301 (2001).
  - <sup>51</sup> Y. C. He, D. N. Sheng and Y. Chen, Phys. Rev. B **89**, 075110 (2014).
  - <sup>52</sup> S. S. Gong, W. Zhu and D. N. Sheng, Sci. Rep. **4**, 6317 (2014).
  - <sup>53</sup> M. P. Zaletel, R. S. K. Mong, F. Pollmann, J. Stat. Mech. **2014**, P10007 (2014).
  - <sup>54</sup> H. Li and F. D. M. Haldane, Phys. Rev. Lett. **101**, 010504 (2008).
  - <sup>55</sup> E. Ardonne, R. Kedem and M. Stone, J. Phys. A:Math. Gen. **38**, 617 (2005).
  - <sup>56</sup> E. Verlinde, Nucl. Phys. B **300**, 360176 (1988).
  - <sup>57</sup> E. Rowell, R. Stong, Z. H. Wang, Comm. Math. Phys. **292**, 343 (2009).
  - <sup>58</sup> P. Fendley, M. P. A. Fisher and C. Nayak, J.Stat.Phys. **126**, 1111(2007).
  - <sup>59</sup> S. Dong, E. Fradkin, R. G. Leigha and S. Nowling, JHEP **05**, 016 (2008).
  - <sup>60</sup> Y. Zhang, T. Grover, A. Turner, M. Oshikawa and A. Vishwanath, Phys. Rev. B **85**, 235151 (2012).
  - <sup>61</sup> Y. Zhang and A. Vishwanath, Phys. Rev. B **87**, 161113(R) (2013).
  - <sup>62</sup> L. Cincio and G. Vidal, Phys. Rev. Lett. **110**, 067208 (2013).
  - <sup>63</sup> W. Zhu, D. N. Sheng and F. D. M. Haldane, Phys. Rev. B **88**, 035122 (2013).
  - <sup>64</sup> M. P. Zaletel, R. S. K. Mong, and F. Pollmann, Phys. Rev. Lett. **110**, 236801 (2013).
  - <sup>65</sup> W. Zhu, S. S. Gong, F. D. M. Haldane and D. N. Sheng, Phys. Rev. Lett. **112**, 096803 (2014).
  - <sup>66</sup> S. Q. Murphy, J. P. Eisenstein, G. S. Boebinger, L. N. Pfeiffer, and K. W. West, Phys. Rev. Lett. **72**, 728 (1994).
  - <sup>67</sup> J. S. Jeong, and K. Park, arxiv.1412.2430v1.
  - <sup>68</sup> S. Geraedts, M. Zaletel, z. Papic, and R. S. K. Mong, arxiv:1502.01340v1.
  - <sup>69</sup> M. R. Peterson, Y.-L. Wu, M. Cheng, M. Barkeshli, Z. H. Wang, S. Das Sarma, arxiv: 1502.02671v1.
  - <sup>70</sup> Zhao Liu, Abolhassan Vaezi, Kyungmin Lee, Eun-Ah Kim

